4 Hund's Metal Physics in the Iron-Based Superconductors

Luca de' Medici
Ecole Supérieure de Physique et Chimie Industrielles de la Ville de Paris
20 rue Vauquelin, 75005 Paris, France

Contents

E. Pavarini, E. Koch, A. Lichtenstein, and D. Vollhardt (eds.)
Understanding Correlated Materials with DMFT
Modeling and Simulation Vol. 15
Forschungszentrum Jülich, 2025, ISBN 978-3-95806-813-1
http://www.cond-mat.de/events/correl25

1 Introduction

Iron-based superconductors (Fe-SC) are one of the many "quantum materials"[1] that are keeping the international research community busy in the recent years. In order to understand, and possibly boost, their superconductivity, a necessary step is understanding their normal metallic phase that turns superconductive below the critical temperature.

This has been characterized as a Hund's metal [1], and this paradigm now applies successfully to many other materials [2].

The name comes from the correlations in the electronic states that are due to the tendency of electrons to distribute themselves on different orbital states with their spins aligned. This energetic convenience, in isolated atoms, is known as a set of rules, the famous "Hund's rules". The fact that these rules have an impact on gases and insulating solids is well known. That they can have strong influence on metallic phases is a much more recent realization [3].

Band theory is the basic approach to crystalline solids, and within it electronic properties of solids are calculated using independent electrons. That is, the electron-electron repulsion is taken into account effectively (differently depending on the specific technique that is used: i.e. Hartree-Fock, any flavor of Density-Functional Theory-DFT, etc.) as an external potential acting on single particles, and the wavefunctions of the eigenstates are Slater determinants of Bloch single-particle eigenfunctions. Each Bloch wavefunction is a plane wave modulating a periodic function which, in some materials, can be quite localized around the lattice sites for the conduction bands. For these materials often band theory is particularly bad in predicting many electronic properties, this being an indication that the independent particle approximation of the wavefunctions is not good enough, and one has to use a more refined scheme. By definition electrons in these materials are called correlated.

The local part of the Bloch wavefunction can be expanded on a local basis, a customary choice being that of (orthonormal) maximally-localized Wannier functions [4] with given s/p/d or f orbital symmetries. In the Slater determinant the weight of the different local configurations (i.e. the coefficient in front of each possible product of local basis functions in the sum) will be dictated by the weights of these orbitals in the Bloch functions. No preference can arise in the wavefunction for specific collective configurations of the electrons on a given site, i.e., high or low total spin, charge or orbital state: these correlations are absent in band theory. Methods that introduce these correlations are needed for modeling these materials correctly, among which indeed are the Fe-SC, as is illustrated in Fig. 1. The plot shows in blue the experimentally measured Sommerfeld coefficient (the slope of the electronic specific heat as a function of temperature at low temperatures) across a range of Fe-SC, each square being a different single-crystal sample. This quantity can be calculated within band theory (DFT) and the results are plotted in black. The discrepancy between theory and experiments is apparent, all the more moving towards the left side of the diagram, indicating an increasing impact of

[1] Quantum materials is an "umbrella term" encompassing materials showing interesting non-trivial quantum properties, among which unconventional superconductivity has certainly a prominent spot.
`https://en.wikipedia.org/wiki/Quantum_materials`

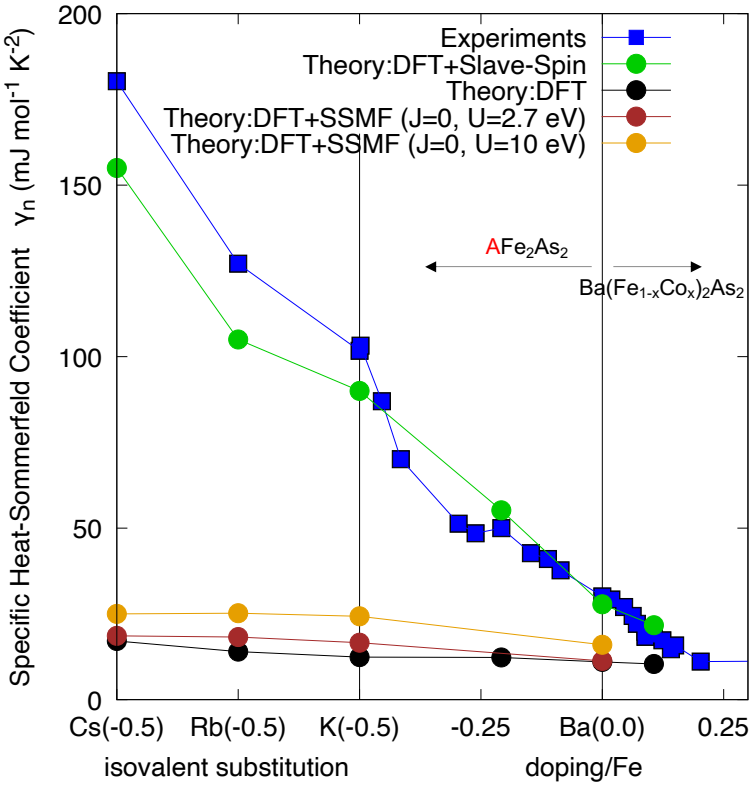

Fig. 1: *Sommerfeld coefficient, i.e., the coefficient γ of the low-T electronic specific heat ($C_V \sim \gamma T + \cdots$) of the normal metallic phases in the "122" family of Fe-based superconductors. Its mother compound, $BaFe_2As_2$ can be electron doped with the substitution of Co for Fe, and hole-doped replacing Ba with K, yielding the level of doping reported on the x-axis. The hole-doped end members AFe_2As_2 (A=K, Rb, Cs) are isovalent. Experimental values are reported in blue, while DFT-GGA results are in black, the discrepancy highlighting the strongly correlated nature of these materials. DFT+Slave-spin mean-field (in green) calculations performed with a single choice of the interaction values ($U = 2.7\,eV$, $J/U = 0.25$) are able to reproduce the whole trend by including dynamical local correlations. Switching off only the Hund's coupling J (brown) makes the results fall back towards the uncorrelated ones, no matter how large (even unphysically large—dark yellow) the value of the Coulomb interaction U is chosen, demonstrating the predominant role of Hund's coupling in these materials.*

the neglected correlations. The results of an approach including them (DFT+Slave-Spin mean-field, reported in green) captures the whole series of experiments instead, proving the point. Neglecting specifically the aforementioned Hund's rules in the approach, even when including the more familiar charge correlations (i.e. the tendency of electrons to avoid packing on the same site, reported in yellow and brown as "J=0") results in a spectacular fall back close to the band-theory results, demonstrating that Hund's physics is the key player here.

In this chapter we will try to break down this calculation to inspect its gears and to gain—also through some simplified models—insight into why and when Hund's physics is important and a material can be rightfully seen as a Hund's metal.[2]

[2]I gave previously a lecture at the Jülich school of 2017 entitled "Hund's metals, explained". Both lectures' subject is Hund's metal physics and they both address its importance in the Fe-SC. I have tried, however, to maintain the information overlap between the two lectures to a minimum, making them maximally complementary.

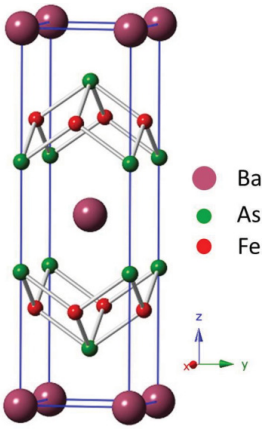

Compound	$a = b$(Å)	c(Å)	z_{As}
$BaFe_2As_2$	3.9625	13.0168	0.3545
KFe_2As_2	3.844	13.916	0.35249
$RbFe_2As_2$	3.873	14.459	0.34748
$CsFe_2As_2$	3.905	15.126	0.34189

Fig. 2: *Structure of the AFe_2As_2 compounds (here A=Ba), and structural parameters determined by X-ray diffraction. (F. Hardy, private communication)*

2 Essentials about Fe-based superconductors

Here an essential outline of Fe-SC will be given, without any attempt of neither a historical account nor a review of the literature (for which two nice starting points are Refs. [5, 6]).

- Fe-SC are materials including planes of Fe atoms forming a square lattice with ligands in the middle of the squares, alternatively slightly above and below the level of the plane. The ligands can be Pnictogens (As, P) or Chalcogens (S, Se, Te), giving rise to the two groups of Iron Pnictides and Iron Chalcogenides, respectively. Several different families exist in these two groups depending on the spacer layers between these planes. Most of the action happens in the Fe-ligand plane, which motivates the common physics of these materials despite their chemical variations. We will focus on the "122" family, taking the name from the stoichiometric formula AFe_2As_2 (where A can be Ba, K, Rb, Cs),[3] where the spacer layer hosts only the cation A (see Fig. 2). Their symmetry is tetragonal (i.e., the conventional unit cell has equal dimensions a=b in the x and y directions, but not in the z direction), with orthorhombic distortions (i.e. $a \neq b$) happening at low temperatures in some cases.

- The striking feature that makes this family extremely interesting is that it can be chemically tuned in a very fine way. Isovalent substitutions (P for As) can be used to apply chemical pressure, while others can be used to tune the electronic density. Using formal oxidation states Ba^{2+} and As^{3-} gives to Iron the valence Fe^{2+}, which since the Fe has the ground state configuration [Ar]$3d^6 4s^2$ means that it will host 6 electrons in the $3d$-orbitals on average. Substituting Fe with Co (but also with Ni) introduces extra electrons, whereas the substitution of Ba with K introduces extra holes, and all the compositions between the stoichiometric $BaFe_2As_2$ and KFe_2As_2 can be obtained, thus providing the very fine phase diagram reported in Fig. 3. Given that the formal oxidation state for the alkaline elements is K^{1+}, the average number of electron hosted on Fe diminishes to 5.5. As said the end member KFe_2As_2 has isovalent siblings with K replaced by Rb or Cs.

[3] And also Na, Ca and Sr which we will not address here.

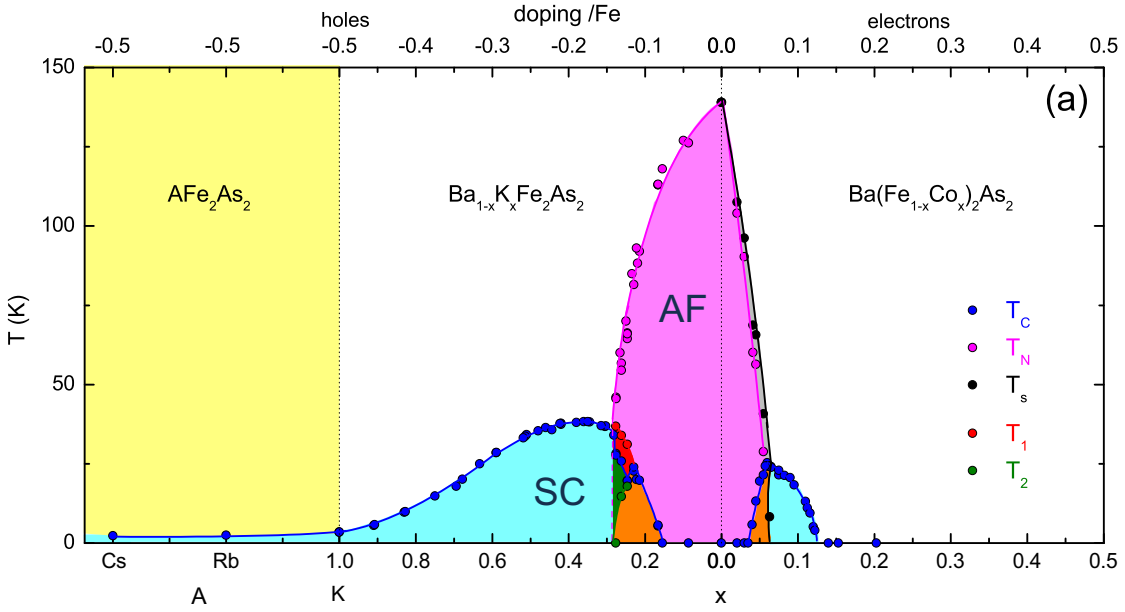

Fig. 3: *Phase diagram of electron and hole-doped $BaFe_2As_2$ (where Fe is formally in the $3d^6$ configuration at stoichiometry), and of the end-members of the family (yellow area, with Fe in the formal $3d^{5.5}$ configuration) AFe_2As_2 (A=K,Rb,Cs). The white/yellow zone of the phase diagram is paramagnetic and metallic, AF indicates a collinear metallic antiferromagnetic phase, SC indicates superconductivity. Other colors indicate coexistent phases. (adapted from [7])*

- In the phase diagram three main phases are present: a metallic "normal" phase for all compounds at high temperatures, turning into an antiferromagnetic metal (with reduced orthorhombic symmetry) or into a superconductor, depending on the composition, below the respective critical temperatures. The metallic phases are standard Fermi liquids, showing, e.g., a T^2 dependence of the resistivity, saturating Pauli magnetic susceptibility and T-linear specific heat (of which the slope is reported in Fig. 1) at low temperature. The maximal critical temperature for superconductivity varies across the families, it tops at ~ 40 K for the 122 family, while the record for a bulk Fe-SC is ~ 56 K for the "1111" family. Monolayer FeSe on a $SrTiO_3$ substrate was reported having $T_c > 65$ K.

3 Modeling Fe-based superconductors

Ab-initio modeling of Fe-SC can be straightforwardly performed within DFT, using the experimental structural parameters determined by X-ray diffraction (reported in Fig. 2). For AFe_2As_2 the Bravais lattice is body-centered, space group $I4/mmm$ in the tetragonal phases (turning to $Fmmm$ in the orthorhombic phases). The bandstructures obtained with the PBE-GGA functional are reported in Fig. 4 (green curves in the right panels). The plots focus on a range of a few eV around the Fermi level, on the conduction bands which are responsible of the electronic properties of these materials and which, as it is visible on the left panels, have mostly a character of Fe $3d$-orbitals.

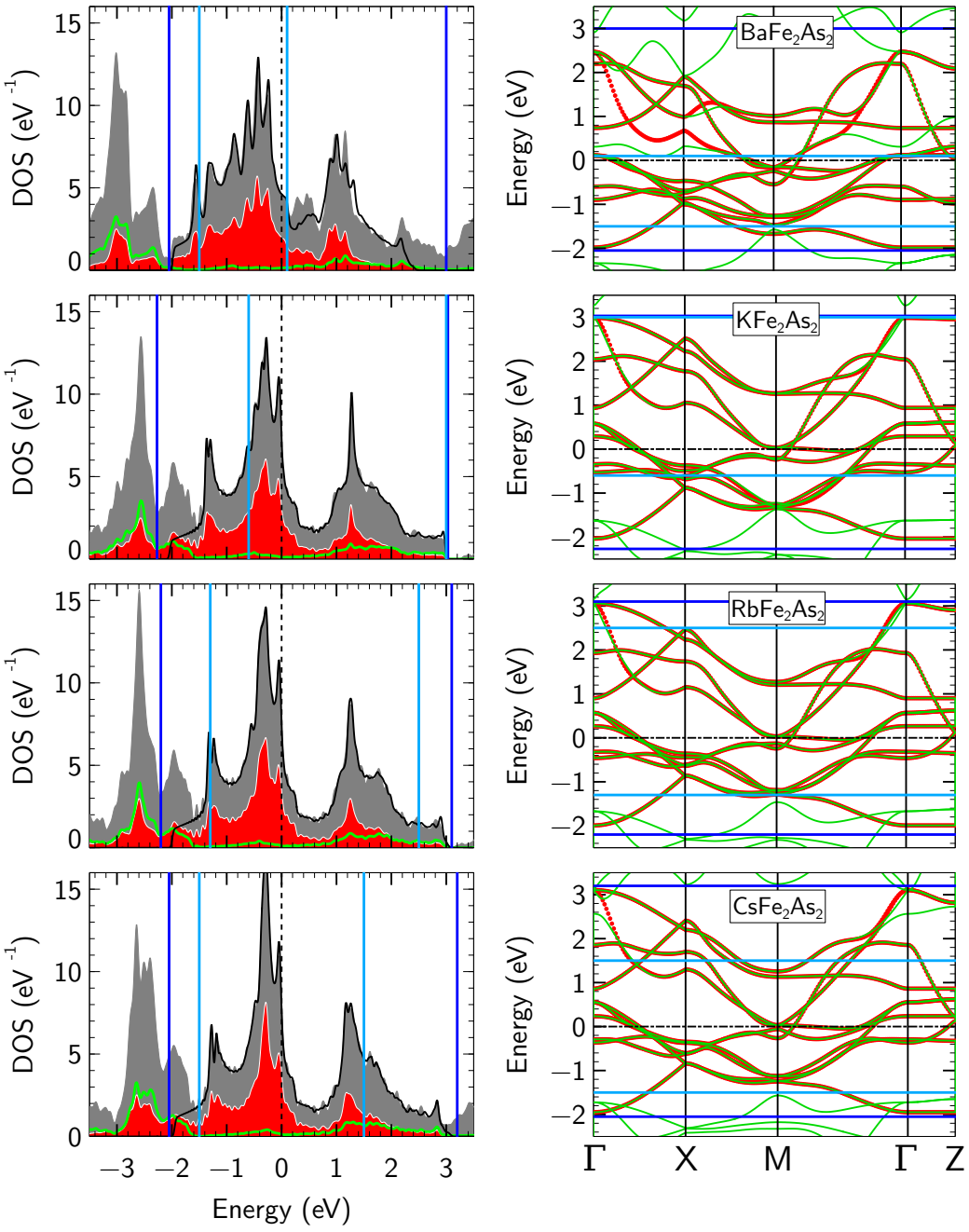

Fig. 4: *Electronic structure and maximally-localized Wannier function fitting of the conduction bands for the main stoichiometric compounds of the 122 family. Right panels: the DFT bandstructure—zoomed in to an energy range of a few eV around the Fermi level—is reported in green on a path in the Brillouin zone of the tetragonal BCC lattice. The fit of these bands with 5 Wannier d-orbitals centered on each Fe atom is drawn in red. Left panels: the total DFT DOS in this energy range is reported in grey. The contribution of each of the two Fe atoms is in red, while that of the As ligands is in green. The black line is the DOS of the tight-binding Wannier model. The dark and light blue lines define the outer and the inner ("frozen") windows for the Wannier90 procedure for obtaining MLWF and the tight-binding model for each compound. (courtesy of Pablo Villar Arribi [8])*

Three main comments are in order, on the DFT bandstructures:

1. Most of the bands have little dispersion in the z-direction (Γ–Z path in these figures), owing to the relatively bi-dimensional nature of these materials. Thus, the resulting Fermi surfaces will have little evolution along z and can be well characterized by looking at their cuts in the k_z=0 plane (path Γ–X–M–Γ). Importantly, the bands in $BaFe_2As_2$ cross the Fermi level around the center of the Brillouin zone Γ and near its corner M, creating there hole pockets and electron pockets, respectively. This *semi-metallic* nature of the mother compounds is shared among all the families of Fe-SC, and is observed in ARPES experiments. The various pockets are similar in size and shape and this creates quasi-nesting conditions boosting the magnetic susceptibility, which explains the arising of the magnetic phases and provides a natural mechanism for unconventional superconductivity mediated by spin fluctuations [5].

   Since the substitution of Ba with alkalines diminishes the electrons in the system the Fermi level moves down in these compounds, making the hole-pockets larger, while the electron pockets essentially empty out and leave little features in the Fermi surface around the M point.

2. Despite the Fermi surfaces matching qualitatively the experiments, the measured dispersion of the conduction bands is much smaller than the calculated bandstructure by at least a factor of 2 to 3. This is a typical sign that dynamical correlations are important, since the dressed quasiparticles replacing the bare electronic excitations of independent electrons have a larger mass and smaller velocity, thus mainly "squeezing" the dispersions around the Fermi level. Moreover it is seen that bands where the Fe t_{2g} (and in particular the d_{xy}) orbital character is dominant are substantially more strongly renormalized than the others, indicating the *selective* strength of the correlations among the different electrons.[4] This band-theory/experiment mismatch is smaller for the electron-doped compounds but larger the more hole doping is introduced. It is strikingly illustrated in the value of the Sommerfeld coefficient γ discussed in the introduction and shown in Fig. 1. Indeed, $\gamma = \pi^2 k_B^2 / 3N^*(E_F)$ is proportional to the density of states (DOS) of the quasiparticles at the Fermi level $N^*(E_F)$, which increases with the aforementioned mass increase due to dynamical correlations. In cases of selective correlations the most correlated electrons can make the DOS very large even in the presence of other much less correlated electrons. For a doping of 0.5 holes/Fe (i.e., for KFe_2As_2 and its isovalent siblings) correlations are very strong and very selective.

3. Taking into account local dynamical correlations, as we will see in the following, does not cure *all* quantitative discrepancies between theory and experiments [1], however. Indeed the Fermi pockets have typically a larger size in calculation than in experiments, and in some cases a pocket is present in the DFT result whereas the band responsible

[4] Both the experimental and the theoretical aspects of the orbital selectivity of Fe-SC's correlation strength were discussed in depth in the lecture of 2017.

for it is seen in ARPES data away from E_F. This mismatch can obviously alter the estimate of many low-energy electronic properties (for example the value of $N^*(E_F)$, the nesting properties, etc.). In semi-metals as the Fe-SC this is a typical outcome of the self-interaction, a known issue of LDA or GGA flavors of DFT, absent in Hartree-Fock. As a matter of fact improving the treatment of the exchange energy beyond standard DFT can cure it and improve the calculation of the Fermi surface and of the related properties (see Ref. [9] and references therein).

In order to include dynamical correlations in the modeling, the electron-electron interaction has to be treated beyond the mean-field level. The (screened) Coulomb interaction decaying quickly with the distance, it is customary to expand it on a basis of localized functions, which is also very efficient in describing the one-body part of the Hamiltonian, since as we mentioned previously the electronic density associated to the conduction bands is quite concentrated around the lattice ions. One such orthonormal basis is that of the maximally-localized Wannier functions (MLWF) that can be optimized so to best parametrize eigenstates and eigenfunctions in the conduction bands of the DFT solution [4]. Their character is mainly Fe-$3d$ as we said, with some contribution from the $4p$-electrons of the ligands. A natural choice is then to use a set of 5 basis functions of d-like symmetry on each Fe ion, and 3 basis functions of p-like symmetry on each ligand ion, a total of 16 functions per unit cell. This p-d ***model*** is more accurate but of greater complexity than the customary ***d-model***, i.e., the alternative choice of introducing only 5 basis functions of d-like symmetry on each Fe ion. These functions cannot be as localized as in the p-d model, but reduce the number of interaction parameters in the model.
Once chosen[5] the basis of Wannier functions $w_m(r-R_i)$ the Hamiltonian of the conduction electrons reads

$$H = \sum_{ijmm'\sigma} t_{ij}^{mm'}\, d^\dagger_{im\sigma} d_{jm'\sigma} + \frac{1}{2}\sum_{ijkl}\sum_{mm'nn'}\sum_{\sigma\sigma'} V_{ijkl}^{mm'nn'}\, d^\dagger_{im\sigma} d^\dagger_{jm'\sigma'} d_{kn'\sigma'} d_{ln\sigma} \tag{1}$$

where $d^\dagger_{im\sigma}$ is the creation operator of an electron with spin σ in the state whose wavefunction is $w_m(r-R_i)$, and

$$t_{ij}^{mm'} = \int d\mathbf{r}\, w_m^*(\mathbf{r}-\mathbf{R}_i)\left(-\frac{\hbar^2}{2m_e}\nabla^2 + V_{\text{eff}}(\mathbf{r})\right) w_{m'}(\mathbf{r}-\mathbf{R}_j) \tag{2}$$

and

$$V_{ijkl}^{mm'nn'} = \int d\mathbf{r} d\mathbf{r}'\, w_m^*(\mathbf{r}-\mathbf{R}_i) w_{m'}^*(\mathbf{r}'-\mathbf{R}_j)\, W(\mathbf{r},\mathbf{r}',\omega{=}0)\, w_n(\mathbf{r}'-\mathbf{R}_k) w_{n'}(\mathbf{r}-\mathbf{R}_l) \tag{3}$$

where $V_{\text{eff}}(\mathbf{r})$ is the effective one-body potential used in the band-theory calculation (e.g. the Kohn-Sham potential in DFT) and $W(\mathbf{r},\mathbf{r}',\omega{=}0)$ is the low-frequency limit of the Coulomb

[5] A technical point is worth stressing for obtaining an optimal basis of MLWF, using, e.g., the publicly available code Wannier90: Two windows of energy need to be defined in order to have a faithful representation of the conduction bands *and* localized basis functions. An outer window encompasses all the bands to be fitted, whereas an inner ("frozen") window enforces the part to be reproduced exactly [4]. In Fig. 4 well-working choices for these windows are indicated by dark and light blue lines respectively for each of the compounds, both in the left and in the right panels. These were used in defining the models we utilize in the following.

interaction $e^2/|\mathbf{r}-\mathbf{r}'|$ screened by all the excitation processes to and within the bands that are not included in this low-energy model. It can be calculated in different frameworks, a customary choice being constrained-RPA approximation (c-RPA). For most Fe-SC, c-RPA calculations were reported in Ref. [10].

Owing to the localized nature of the Wannier functions and to the rapid decay of the screened interaction with distance, a common simplifying choice is to retain only the local terms of the interaction, i.e., $V^{mm'nn'} \equiv V^{mm'nn'}_{ijkl}\delta_{ij}\delta_{jk}\delta_{kl}$. This gives rise to a *multi-orbital Hubbard model*.

Among the matrix elements of the local interaction a typical choice (exact in some limits, e.g., in the presence of a large cubic field splitting that allows one to treat the three t_{2g} orbitals separately from the two e_g orbitals [3]) is to retain only the terms containing the integrals $U_{mn} \equiv V^{mmnn}$, and $J_{mn} \equiv V^{mnmn}$ (with $n \neq m$) and, defining U as the average of the U_{mm} and J the average of the J_{mn} for $n \neq m$ over the orbitals, to finally write down the *Kanamori interaction*[6]

$$\begin{aligned} H_{\text{int}} &= U\sum_{im}\tilde{n}_{im\uparrow}\tilde{n}_{im\downarrow} + (U-2J)\sum_{im\neq m'}\tilde{n}_{im\uparrow}\tilde{n}_{im'\downarrow} + (U-3J)\sum_{im<m',\sigma}\tilde{n}_{im\sigma}\tilde{n}_{im'\sigma} \\ &- J\sum_{im\neq m'} d^\dagger_{im\uparrow}d_{im\downarrow}\,d^\dagger_{im'\downarrow}d_{im'\uparrow} + J\sum_{im\neq m'} d^\dagger_{im\uparrow}d^\dagger_{im\downarrow}\,d_{im'\downarrow}d_{im'\uparrow}, \end{aligned} \tag{4}$$

where $n_{im\sigma} \equiv d^\dagger_{im\sigma}d_{im\sigma}$ is the number operator and $\tilde{n}_{im\sigma} \equiv n_{im\sigma}-\frac{1}{2}$ its particle-hole symmetric version.[7] J being the parameter favoring the spin alignment and the distribution of electrons on different orbitals, is called the "Hund's coupling".

Solving and exploring this Hubbard-Kanamori model for the Fe-SC is still a formidable task. However it can be done in several frameworks. Indeed several approaches and levels of perturbation theory in the interaction are the methods of choice, able to explore instabilities of the DFT bandstructures towards the various broken symmetry phases found in the phase diagrams of these materials. The strength of the correlations, however, as we have previously highlighted, casts some doubts on the quantitative (and in several important cases qualitative) validity of such approaches. Also, typically calculated values of U range from 2.5 to 4.2 eV (J is typically smaller, i.e., $J/U = 0.12\ldots0.15$) which is of the order of the DFT bandwidth (see, e.g., Fig. 4). We here expose the results of non-perturbative methods, thus not assuming a small interaction as a starting point in any way.

One such methods is Dynamical Mean-Field Theory (DMFT), presented in this book in the chapter by Eva Pavarini. Here we will rather expose the Slave-spin mean-field (SSMF) method, which can be seen as a simpler dynamical mean-field technique providing orbital-selective band renormalization and giving direct analytical access on the mechanisms behind it.

[6] Here it is seen that the off-diagonal elements of U_{mn} are not used. Indeed it is found that they are typically close to $U-2J$ (an exact relation in some cases) which is then taken as a further simplifying assumption.

[7] This form of the interaction implies a shift of the chemical potential, of no physical meaning. A shift of the chemical potential is implied anyway because of the double counting of the interaction already included in $V_{\text{eff}}(r)$, which is not an issue in the d-model formulation for this reason.

4 Slave-spin mean-field

In the slave-spin representation, the original fermionic model is mapped on an auxiliary model having both fermions and spin variables on a lattice. That is, to every local electronic one-particle state (created by $d^\dagger_{im\sigma}$) are associated in the auxiliary, larger Hilbert space, both a fermionic state (created by $f^\dagger_{im\sigma}$) and a spin-1/2 variable, of z-component $S^z_{im\sigma}$ (and flipped by $S^\pm_{im\sigma}$). They both carry the same indices of the original d fermion, and the slave-spin has no special relation—and should not be confused—with the physical spin. An occupied local state $|1\rangle_d$ in the original space is then associated, in the auxiliary Hilbert space, to the direct product of the occupied state for the corresponding f fermion and to the "up" (that we indicate with 1) state of the associated "slave"-spin $|1\rangle_f|1\rangle_s$. Likewise an empty d-state $|0\rangle_d$ is associated to the empty fermionic state and the "down" (that we indicate with 0) state of the slave spin $|0\rangle_f|0\rangle_s$. These "physical" states satisfy the operatorial relation

$$f^\dagger_{im\sigma} f_{im\sigma} = S^z_{im\sigma} + \frac{1}{2}, \tag{5}$$

which can be used to distinguish them from the remaining combinations $|1\rangle_f|0\rangle_s$ and $|0\rangle_f|1\rangle_s$ which have no physical counterpart.

This is apparently a complication, but it turns out that approximations performed on the larger space can be less severe than if applied directly to the original system.

The operators of the original space are mapped on operators having the same matrix elements between the physical states of the larger space, while their action on the unphysical states can be chosen freely, in principle. In practice this freedom is used to gauge approximated treatments, e.g., to reproduce known limits and possibly yield the most physical results.

Hence the number operator $n_{im\sigma} = d^\dagger_{im\sigma} d_{im\sigma}$ can be equivalently mapped into the number operator for the pseudo-fermions $n^f_{im\sigma} = f^\dagger_{im\sigma} f_{im\sigma}$ or into $S^z_{im\sigma} + \frac{1}{2}$, which, because of Eq. (5), gives the same result by construction on the physical states. The interaction Hamiltonian Eq. (4) then, for which we customarily consider only the density-density terms,[8] can be written in terms of the S^z operators only

$$H^s_{\text{int}} = \sum_i H^s_{\text{int}}[i] = U \sum_{im} S^z_{im\uparrow} S^z_{im\downarrow} + (U-2J) \sum_{im\neq m'} S^z_{im\uparrow} S^z_{im'\downarrow} + (U-3J) \sum_{im<m'\sigma} S^z_{im\sigma} S^z_{im'\sigma}. \tag{6}$$

The one-body part instead involves both slave-spins and pseudofermions, since the off-diagonal destruction (creation) operator $d^{(\dagger)}_{im\sigma}$ is expressed by $f^{(\dagger)}_{im\sigma} O^{(\dagger)}_{im\sigma}$. The general form of the $O_{im\sigma}$ operator is $O_{im\sigma} = S^-_{im\sigma} + c_{im\sigma} S^+_{im\sigma}$, where $c_{im\sigma}$ is an arbitrary gauge embodying the aforementioned freedom. We choose $c_{im\sigma} = \frac{1}{\sqrt{\langle \hat{n}^f_{im\sigma}\rangle_f (1-\langle \hat{n}^f_{im\sigma}\rangle_f)}} - 1$, which, within the present mean-field approximation, can be shown to reproduce the non-interacting limit. Then the total Hamiltonian of our model in the auxiliary Hilbert space reads $H = H_0 + H^s_{\text{int}}$ with

$$H_0 = \sum_{i\neq jmm'\sigma} t^{mm'}_{ij} f^\dagger_{im\sigma} f_{jm'\sigma} O^\dagger_{im\sigma} O_{jm'\sigma} + \sum_{im\sigma} \varepsilon_m f^\dagger_{im\sigma} f_{im\sigma}, \tag{7}$$

[8] Using the full Kanamori form, thus including the spin-flip and pair-hopping terms that we here neglect, does not alter qualitatively any of the analysis or conclusions exposed in this chapter. The differences are merely quantitative ones.

where we have singled out the local terms in the one-body part of Eq. (1) as $t_{ii}^{mm'} = \varepsilon_m \delta_{mm'}$.

The mapping is thus far exact if we could project out all unphysical states strictly enforcing the constraint Eq. (5). In the SSMF scheme three approximations are instead performed. First, we mean-field decouple slave-spin and pseudofermion so that we are left with a non-interacting fermionic Hamiltonian, and a lattice spin model where several slave-spins interact on site and are also coupled to the slave-spins of neighboring sites. Second, we perform a mean-field decoupling of the slave-spin lattice system in the spirit of a Weiss mean-field, and thus we are left with a single-site spin Hamiltonian in an effective field. Third, we treat the constraint on average, with site-independent (and spin-independent, since we address the paramagnetic phases here) Lagrange multipliers λ_m, adjusted so that $\langle n_{m\sigma}^f \rangle = \langle S_{m\sigma}^z \rangle + \frac{1}{2}, \forall i, m, \sigma$. Details of this procedure can be found, e.g., in Ref. [11] and references therein.

The resulting mean-field Hamiltonian is $H - \mu N = H_s + H_f - \mu N$, with

$$H_f - \mu N = \sum_{i \neq j m m' \sigma} \sqrt{Z_m Z_{m'}}\, t_{ij}^{mm'}\, f_{im\sigma}^\dagger f_{jm'\sigma} + \sum_{im\sigma} (\varepsilon_m - \lambda_m + \lambda_m^0 - \mu) f_{im\sigma}^\dagger f_{im\sigma}\,, \tag{8}$$

and $H_s = \sum_i H_s^i$ with

$$H_s^i = \sum_{m\sigma} \big(h_m O_{m\sigma}^\dagger + H.c.\big) + \lambda_m \big(S_{m\sigma}^z + \frac{1}{2}\big) + H_{\text{int}}^s[i]\,, \tag{9}$$

where the self-consistent parameters are

$$Z_m = |\langle O_{m\sigma} \rangle|^2, \tag{10}$$

$$h_m = \sum_{j \neq i, m'} t_{ij}^{mm'} \sqrt{Z_{m'}} \langle f_{im\sigma}^\dagger f_{jm'\sigma} \rangle \tag{11}$$

$$\lambda_m^0 = h_m \sqrt{Z_m}\, \frac{2\langle \hat{n}_m^f \rangle - 1}{\langle \hat{n}_m^f \rangle \big(1 - \langle \hat{n}_m^f \rangle\big)} \tag{12}$$

the latter being a shift due to the mean-field procedure, which reduces to λ_m, and thus cancels it, in the non-interacting limit [11].

Solving these equations iteratively until convergence yields the renormalized quasiparticle Hamiltonian Eq. (8), the bandstructure of which can be compared with the quasiparticle bands measured in ARPES. In particular the orbitally-resolved quasiparticle weight Z_m is the inverse of the orbitally-resolved mass enhancement, and $\varepsilon_m - \lambda_m + \lambda_m^0$ can be seen as a renormalized local orbital energy.

The slave-spin Hamiltonian is still a many-body Hamiltonian that can be used to calculate local correlation functions, here we will see the (z component of the) total local magnetic moment $\Big\langle \big(\sum_m (S_{im\uparrow}^z - S_{im\downarrow}^z) \big)^2 \Big\rangle$.

5 Hund's metal physics

Application of the SSMF to the multiorbital Hubbard models[9] for $A\mathrm{Fe_2As_2}$ with A=Ba, K, Rb, and Cs leads to the results reported in Fig. 5. All the plotted quantities show a clear crossover as a function of U between a weak-coupling and a strong-coupling behavior.
For the lower range of U all the quasiparticle weight Z_m are grouped, weakly dependent on U and barely smaller than 1, their non-interacting value. Analogously, the orbital-resolved mass enhancements, which are exactly their inverse, lie barely above 1 for the whole range. Also the renormalized orbital energies evolve smoothly and the local magnetic moment remains near its small non-interacting value.
All quantities change rapidly around the crossover value of U, and above it one sees a completely different behavior: The Z_m have spread and dropped to small values below (some way below) 0.5, and correspondingly the mass-enhancements are very selective and reach very high values (extremely high for the t_{2g} orbitals and in particular d_{xy}); the renormalized orbital energies have rearranged and now are very close to one-another, while the local magnetic moment has risen and is now very close to its saturation value 5/2. This behavior is the *Hund's metal*.
It is to be noted that the crossover is sharper and happens earlier for the alkaline compounds A=K, Rb, Cs than for $\mathrm{BaFe_2As_2}$. This is mainly due to the difference in the average electron density. As said the alkaline compounds host 5.5 electrons/Fe on average while $\mathrm{BaFe_2As_2}$ has 6 electrons/Fe (and indeed the chemical potentials in the calculations are adjusted so to keep these densities at all interactions). The sharpness of the crossover culminates at half-filling where it converges with the Mott transition. This implies that the Hund's metal is a zone at U larger than the U_c for the Mott transition at half-filling that can be entered both increasing the interaction strength and reducing the doping towards half-filling. In other words the Hund's metal is the doped Mott insulator in presence of sizeable Hund's coupling.
This behavior is clearly understood when analyzing the same features in a 5-orbital Hubbard-Kanamori model of featureless simplified bands (i.e. ε_m=0 for all orbitals and $t_{ij}^{m,m'} = t\,\delta_{m,m'}$ for i nearest neighbor of j on an infinitely-dimensional Bethe lattice, that has a semicircular DOS of half-bandwidth D=$2t$). As visible in Fig. 6, the characteristic crossover [2, 3] to the Hund's metal reported for all integer fillings from n=8.0 to n=5.0 (half-filling)[10] clearly becomes sharper the more half-filling is approached, and is obviously connected to the Mott transition at half-filling (yellow sharp drop). This strong-correlation behavior being connected to the prevalence of high-spin local configurations favored by J, as outlined previously, it is instructive to plot the relative weight of these configurations compared to the others. Indeed for $U/D = 3.0$ and $J/U = 0.25$ it is visible that the high-spin configurations of each sector dominate (i.e. compared to the other configurations with the same number of electrons), and all the more the closer the system is to half-filling.

[9] In these calculations as a function of U a fixed ratio $J/U = 0.25$ was kept. Indeed, it was shown [12, 13] that the physical results for the Kanamori interaction with $J/U = 0.12 \div 0.15$ as estimated by c-RPA are best reproduced in SSMF increasing the ratio to $J/U = 0.25$.

[10] The model being particle-hole symmetric the curves are also representative of the filling between n=2.0 and n=5.0.

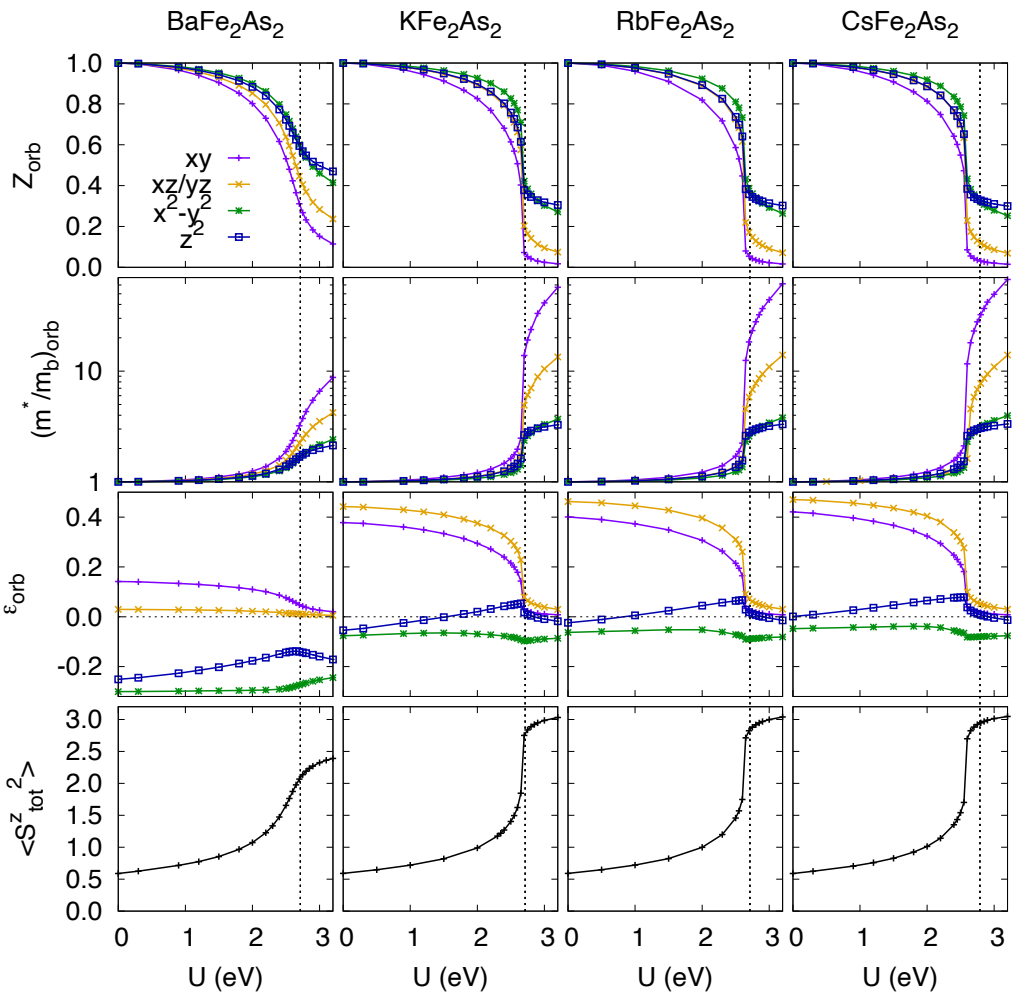

Fig. 5: *Slave-spin mean-field results for AFe_2As_2 with A=Ba, K, Rb, Cs as a function of the interaction strength U (for J/U=0.25). From top to bottom rows: orbitally-resolved quasiparticle weights Z_m, orbitally-resolved mass enhancements $(m^*/m_b)_m = 1/Z_m$ (log scale), renormalized orbital energies and z-component of the local magnetic moment. A clear crossover from a normal metal to the Hund's metal behavior is visible just below the dashed line, which marks the interaction value (close to the one calculated in c-RPA) used for the calculations reported in Fig. 1. The crossover is sharper and happens faster in the calculations for the alkaline compounds (5.5 electrons/Fe) than for $BaFe_2As_2$ (6 electrons/Fe), owing to the influence of the half-filled Mott insulator. (courtesy of Pablo Villar Arribi [8])*

It is clear that both for the realistic calculations and for those in the idealized model, Hund's coupling triggers a behavior where the local high-spin configurations prevail and the quasiparticle weight becomes small (and the mass enhancement large) and selective, all the more for filling near half, but *only* for values of the interaction strength larger than the critical value for the Mott transition at half-filling. It is worth noticing that the Mott insulating states at all the other fillings play very little role in the zone of the phase diagram we are discussing (where the interaction strength U is of the order of the bandwidth or even smaller), relevant to the Fe-SC, because they are sent at much higher critical U values. Conversely the role of the Mott insulator at half filling is clearly dominant, and it seems to act as a catalyst for the Hund's metal, amplifying its features with its proximity.

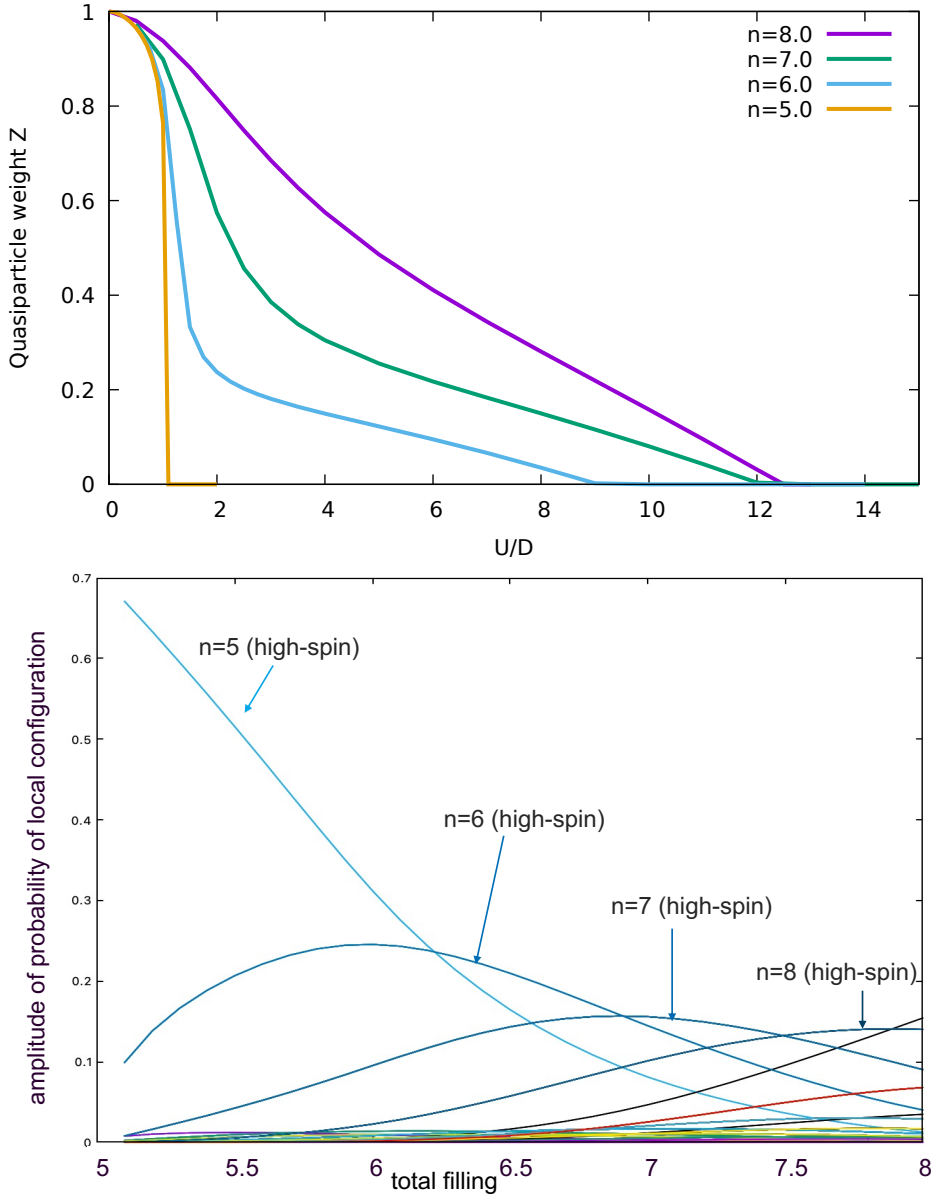

Fig. 6: *5-orbital Hubbard Kanamori model with $J/U = 0.25$. Upper panel: quasiparticle weight Z as a function of the interaction strength U for the integer fillings between half-filling (n=5.0) up to 8 electrons per site, showing the increasing sharpness of the crossover with the proximity to the Mott transition at half-filling. Lower panel: relative weight of the high-spin configuration with the indicated number of electrons in the ground state of the slave-spin Hamiltonian as a function of the filling of the system for $U/D = 3.0$. The weights for all other configurations are also plotted in this graph, most being indistinguishable from the x-axis. (adapted from [14])*

But why is it so? Why is Hund's coupling so efficient in inducing a Mott insulator at half-filling and why are correlations in its proximity so much stronger than at J=0? We can gain this insight by inspecting a few analytical results that can be obtained within SSMF in these idealized models.

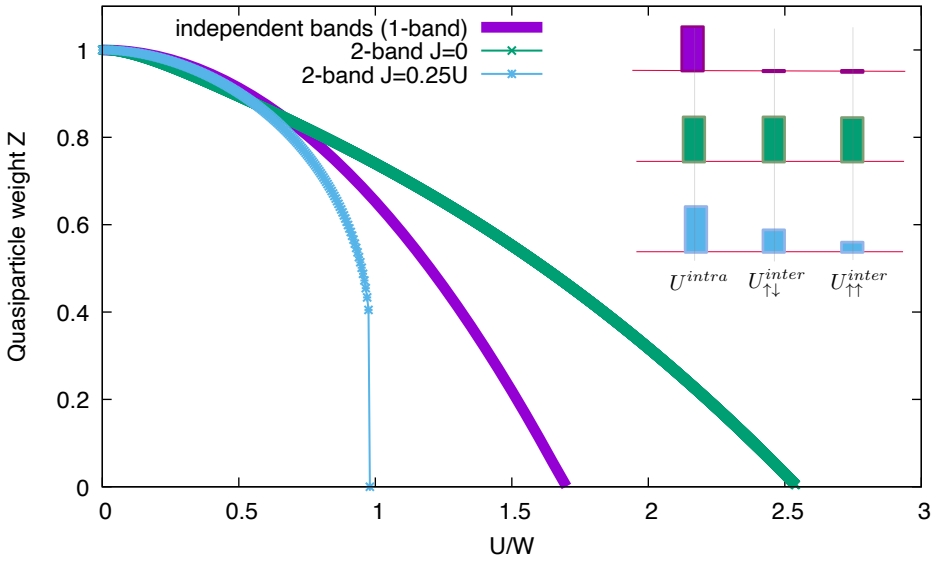

Fig. 7: *Mott transition in the half-filled Hubbard model studied with SSMF (or equivalently Gutzwiller approximation or slave-boson mean-field). Independent bands (purple line) compared with two bands in absence (green) and in presence (light blue) of Hund's coupling J. It might surprise that at strong coupling the second case is less correlated then the first, and the third more correlated than the second, despite the opposite overall trend in the inter-orbital interaction strength (columns sketched on the right). [14]*

6 The working mechanism of Hund's induced correlations

The counter-intuitive nature of Hund's induced correlations can be illustrated by the following simplified paradoxical puzzle, summarized by Fig. 7. Let's imagine a half-filled multi-orbital Hubbard band with featureless bands (as before we can take a semi-circular DOS of bandwidth $W = 2D$, i.e., $D(\varepsilon) \equiv \frac{2}{\pi D}\sqrt{(1-(\frac{\varepsilon}{D})^2)}$) and no inter-orbital hopping.

- If all inter-orbital interaction is switched off too one obtains a collection of single-band Hubbard models, not talking to each other. Their behavior, in particular with respect to the Mott transition will be that of a one-band model (purple line in the figure). Its critical coupling for the Mott transition in SSMF (and in Gutzwiller approximation or slave-boson mean-field) is $U_c = -16\bar{\varepsilon}$, where $\bar{\varepsilon}$ is the bare delocalization ("kinetic") energy at half-filling, i.e., $\bar{\varepsilon} \equiv \int_{-D}^{0} d\varepsilon\, \varepsilon\, D(\varepsilon) \simeq -0.2122D$. As visible in the figure this gives $U_c \simeq 3.4\, D \simeq 1.7\, W$.

- Let's now *turn on* the interaction between the different orbitals. Let's focus for simplicity on the two-orbital case. At J=0 the electrons in the two orbitals will add to their intra-orbital repulsion U and inter-orbital repulsion U to electrons in the other orbital irrespectively of their spin orientation. One might naively expect that this additional repulsion makes the system more correlated. This is however not the case: as visible in the figure (green line) the quasiparticle weight lies systematically above that of independent bands for moderate to strong interactions, and the Mott transition happens at much larger $U_c \simeq 2.5W$!

- Even more puzzling, let's now *reduce* the inter-orbital interaction compared to the intra-orbital one, and even more so for electrons with parallel spins. This is exactly what is done for finite Hund's coupling J/U. Again one might expect this reduction in the electronic repulsion to de-correlate the system, but one finds the opposite. The quasiparticle weight lies below the one for $J{=}0$ at moderate to strong interactions, and the Mott transition happens precipitously at a much smaller $U_c \simeq W$!

The puzzle is solved by the explicit calculation of U_c, that can be effected analytically in SSMF for any number M of orbitals both for $J{=}0$ and finite J. It turns out that a naive balance between bare kinetic energy and interaction strength is not enough to understand the degree of correlation of the system. The energy and degeneracy of local multiplets and the processes available for fluctuating between different charge states are of importance instead, and these are tuned by Hund's coupling, as we are going to see now.

In the slave-spin mean-field approximation[11] a Mott insulator is a solution in which $Z_m = 0$. By the self-consistency equation Eq. (11), this implies $h_m = 0$. Thus in proximity of a Mott insulator a perturbative treatment in h_m of the slave-spin problem can be performed.
In the half-filled, particle-hole symmetric case with no crystal-field splitting (i.e. $\varepsilon_m = 0$), $\mu{=}\lambda_m{=}\lambda^0_m{=}0$ and $c_m{=}1$. Then the unperturbed Hamiltonian is simply $H^s_{\text{int}}[i]$ from Eq. (6).
At $T{=}0$ we only need the ground state of this Hamiltonian, which will have a different degeneracy d_0 depending on the value of J, so later on we will distinguish the $J{=}0$ from the finite J case. The perturbing Hamiltonian is

$$V \equiv H^i_s - H^s_{\text{int}}[i] = 2h \sum_{m\sigma} 2S^x_{m\sigma} = 2h \sum_{m\sigma} \left(S^+_{m\sigma} + S^-_{m\sigma}\right), \tag{13}$$

where $h \equiv h_m$ is here equal for all the M orbitals. It simply flips any of the slave-spins.
It removes the ground state degeneracy at the second order in h (the perturbation has no matrix elements within the degenerate subspace), and in order to obtain the "correct" unperturbed ground state $\left|\phi^{(0)}_0\right\rangle$ (the one to which the perturbed ground state tends for $h \to 0$) one has to diagonalize the matrix $H' \equiv V\left(E_0{-}H^s_{\text{int}}\right)^{-1}V$ in the degenerate subspace, where E_0 is the unperturbed ground state energy. The ground state ket will have a correction at the linear order instead, which according to standard perturbation theory reads: $\left|\phi^{(1)}_0\right\rangle = \left|\phi^{(0)}_0\right\rangle + \sum_{|s\rangle\neq|\phi_0\rangle} \langle s|\left(E_0{-}H^s_{\text{int}}\right)^{-1}V\left|\phi^{(0)}_0\right\rangle|s\rangle$.
The self-consistency condition Eq. (11) is needed to determine the solution of the mean-field equations, and in the present case simplifies to

$$h = \sqrt{Z_m}\bar{\varepsilon}\,. \tag{14}$$

$\sqrt{Z_m} = \left\langle 2S^x_{m\sigma}\right\rangle$ is itself a function of h, and this relation determines the self-consistent value of h for a given set of physical parameters. The critical parameters for the Mott transition are found when the solution goes to $h{=}0$, so the linear term in h is enough.

[11] In the presentation of the slave-spin analytical calculations we follow closely the Appendix of Ref. [15]

A particularly relevant and insightful quantity to calculate then is

$$4hM\langle 2S^x_{m\sigma}\rangle = \langle V\rangle = \langle \phi_0^{(1)}|V|\phi_0^{(1)}\rangle = 2\langle \phi_0^{(0)}\big|V\big(E_0{-}H^s_{\rm int}\big)^{-1}V\big|\phi_0^{(0)}\rangle, \tag{15}$$

(where we used explicitly the fact that $\langle \phi_0^{(0)}|V|\phi_0^{(0)}\rangle = 0$).
Eq. (15) illustrates that $\langle V\rangle$ (and thus $\langle 2S^x_{m\sigma}\rangle$) counts the number of ways in which flipping any two slave-spins brings the ground state into (a state having overlap with) itself, weighed by $2/(E_0{-}E_S)$, twice the inverse of the (negative) energy difference between the ground state and the intermediate excited state.
In physical terms this tracks the number of processes by which a particle can hop onto a neighboring site and back to any of the spin-orbitals still turning the ground state into (having overlap with) itself [16]. This is in strict analogy with the perturbative arguments determining Kondo coupling of an impurity in a bath which through dynamical mean-field theory describes the itinerancy of particles in a lattice model [3].
Now these processes are enhanced in presence of large degeneracy of the energy multiplets. We illustrate this in the following by comparing the case at $J{=}0$ with that for finite J.

- *$J{=}0$, $SU(2M)$ symmetry*

At $J=0$, up to a constant shift, $H^s_{\rm int}[i] = U/2\big(\sum_{m\sigma} S^z_{m\sigma}\big)^2 = U/2\big(S^z_{tot}\big)^2$. The system has an even number $2M$ of slave-spins on each site, hence any state with $S^z_{tot}=0$ is a ground state. Owing to the $SU(2M)$ symmetry of the $J=0$ problem, there are $d_0 = \binom{2M}{M}$ such states ($|S^z_{tot}{=}0;\, l\,\rangle$, for $l{=}1\dots d_0$) , corresponding to the number of ways to take half of the $2M$ slave-spins up and half down. Physically this corresponds to the ways of putting M particles in $2M$ spin-orbitals, owing to the half-filling of the system.
All the states with one flipped spin are $U/2$ higher in energy from the ground state and hence one can diagonalize $H' = -2V^2/U$. The lowest-energy eigenstate of the restriction of H' to the unperturbed degenerate manifold is

$$\big|\phi_0^{(0)}\big\rangle = \frac{1}{\sqrt{d_0}}\sum_{l=1}^{d_0}\big|S^z_{tot}{=}0;\, l\,\big\rangle \tag{16}$$

i.e., the linear combination of all the degenerate basis states in the ground state manifold with all plus signs. This can be easily checked by inspection. Indeed H' flips down any of the M spins pointing up, and then flips up any of the now $M{+}1$ spins pointing down. The analogous process takes place starting with a flip up. This makes $2M(M{+}1)$ possible processes. The fact that *all of the* d_0 degenerate basis states with M spins up and M spins down are included in the linear combination ensures that all these "exchange" processes are active. The plus signs in the linear combination also ensures that all the corresponding $-U/2$ contributions add up, generating the lowest possible energy.
This, by inserting $|\phi_0^{(0)}\rangle$ into Eq. (15) results in

$$\langle 2S^x_{m\sigma}\rangle = -\frac{8h}{U}(M{+}1) \tag{17}$$

- *$J\neq 0$ with density-density interaction, Z_2 symmetry*

For $J \neq 0$, $H^s_{\text{int}}[i]$, Eq. (6), splits the manifold with $S^z=0$ and for the case of density-density only interaction the ground state is *only two times degenerate*.[12] The two degenerate states are $|1,\dots,1,0,\dots,0\rangle$, with all M slave spins corresponding to spin-orbitals $m\uparrow$ —in our ket notation the first M of all the $2M$ slave-spins—pointing "up" (1, in our notation) and the remaining ones pointing "down" (0 in our notation), or the inverse $|0,\dots,0,1,\dots,1\rangle$.
The excitation energy of the states that can be reached by flipping one spin starting from the ground state and flipped back to it is $U_{\text{eff}}/2$ with $U_{\text{eff}} = U + (M-1)J$, so the matrix to be diagonalized to find the "correct" unperturbed ground state is the restriction of $H' = -2V^2/U_{\text{eff}}$.
This degeneracy is split at order h^{2M}, but the "correct" unperturbed ground state is still the linear combination of these two basis states with the plus sign

$$\left|\phi_0^{(0)}\right\rangle = \frac{1}{\sqrt{2}}\big(|1,\dots,1,0,\dots,0\rangle + |0,\dots,0,1,\dots,1\rangle\big). \tag{18}$$

However to leading order h^2 only $2M$ processes are active: those flipping twice a given slave spin. Thus inserting $\left|\phi_0^{(0)}\right\rangle$ into Eq. (15) gives

$$\langle 2S^x_{m\sigma}\rangle = -\frac{8h}{U_{\text{eff}}} = -\frac{8h}{U+(M-1)J} \tag{19}$$

which, for any $M \geq 2$, is much smaller than in the $J=0$ case.
Using this in the self-consistency condition Eq. (14) and eliminating h one can solve for the critical interaction for the Mott transition

$$U_c = \begin{cases} 8(M+1)|\bar{\varepsilon}|, & J=0, \quad \forall M \quad (\text{including } M=1) \\ 8|\bar{\varepsilon}| - (M-1)J & J\neq 0 \quad \text{and} \quad M\geq 2 \end{cases} \tag{20}$$

the latter relation being equivalent to say that to $U_c^{\text{eff}} = 8|\bar{\varepsilon}|$.

These results illustrate our point that the degeneracy of the ground state and of the multiplets visited by charge fluctuations enhance the itinerancy, through the activation of extra hopping channels.
This is the reason for the reduction of correlations in a multi-orbital system in absence of Hund's coupling, indeed in that case the U_c grows with the number of orbitals M.
Hund's coupling changes the situation, and increases the correlation strength for two reasons, as obvious comparing the expressions eqs. (17) and (19):

1. it reduces the number of processes contributing to $\langle V\rangle$ (and thus to $\langle 2S^x_{m\sigma}\rangle$), thus eliminating the $M+1$ prefactor,

2. increases the value of U^{eff}, thus increasing the cost for charge fluctuations, and weighing more the denominator in Eq. (19).

[12] In the case of full Kanamori interaction, including the spin-flip and pair-hopping terms, the degeneracy of the ground-state multiplet is not as reduced. However it is still much smaller than for the $J=0$ case. Thus our treatment, albeit quantitatively not exact, is qualitatively representative also of the Kanamori case.

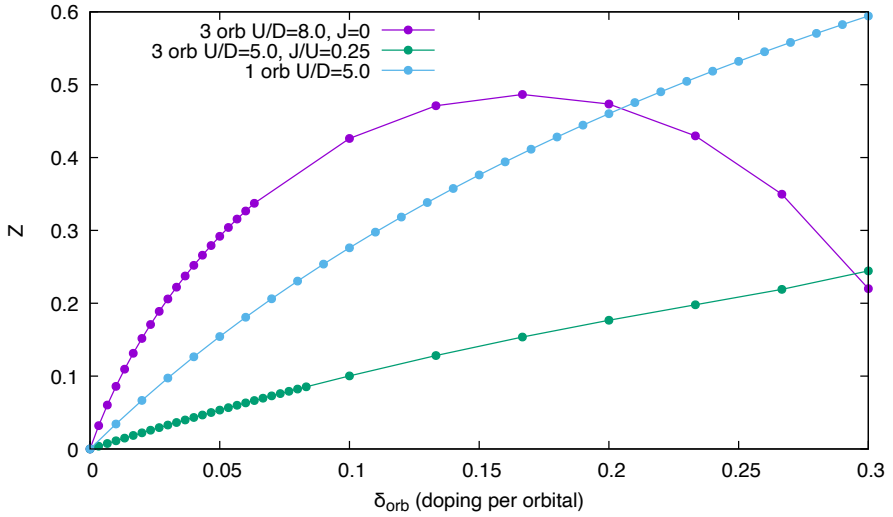

Fig. 8: *Doping dependence of the quasiparticle weight for doped half-filled Mott insulators: a 3-orbital Hubbard model with and without Hund's coupling J is compared to the single-band case. Visibly, the multi-orbital case with J=0 is less correlated than the single-band case (even for the considerably larger value of U, chosen so to be well beyond $Uc(J{=}0)$). The multi-orbital case in presence of J is much more strongly correlated than both (even more so when considering the* total *doping and not the doping* per orbital *as shown here). The parallel with the behavior of Z at half-filling as a function of $U < U_c$ plotted in Fig.7 is obvious, for the reasons explained in the main text. (adapted from [14])*

These two aspects were explored from DMFT perspective in Ref. [17]. Here we have shown explicitly the mechanism at work through an analytical calculation, showing how the many-body hopping channels participate to the geometrical factor enhancing or reducing U_c. In this respect it is worth mentioning that away from integer fillings other than half the reason 1 above still applies, while reason 2 does not. In fact $U^{\rm eff} = U{+}3J$ in these cases, thus rather pushing U_c away. Nevertheless in most of the U range correlations are found enhanced because of reason 1.

A further interesting point is that here with the same formalism the dependence of the quasi-particle weight Z on the doping for a doped Mott insulator can be obtained. After a similar calculation and for the same reasons as above one gets

$$Z = \begin{cases} \frac{M+1}{\sqrt{1-U_c/U}}\,\delta_{\rm orb}, & J=0, \quad \forall M \quad (\text{including } M{=}1) \\ \frac{1}{\sqrt{1-U_c^{\rm eff}/U^{\rm eff}}}\,\delta_{\rm orb} & J\neq 0 \quad \text{and} \quad M\geq 2 \end{cases} \tag{21}$$

where $\delta_{\rm orb} = \delta/M$ is the *doping per orbital*.
Typical behaviors are illustrated in Fig. 8 for a three-orbital Hubbard model. As it happens, for the half-filled metal, also in the present case of a doped Mott insulator, for the same conditions of doping, the multi-orbital case with J=0 is much less correlated than the single-band case. The multi-orbital model in presence of J is instead much more correlated than the single band case. It is to be noted, by the way, that the plot compares the models at the same doping *per orbital*. As a function of the total doping in the model the multi-orbital case is then even more strongly correlated than it appears on this plot, compared to a typical single-band doped Mott insulator.

Thus overall not only the half-filled Mott insulating state is strongly favored by Hund's coupling, given the strong reduction of U_c due to J, but also the correlations, when doping this Mott insulating state, are enhanced and decrease more slowly with doping than in the case without J. This is, in essence, the reason why Hund's metal physics is so relevant for Fe-SC, and all the more the closer to half-filling they are, as anticipated at the end of section 5.

7 Conclusions

In this lecture we have discussed the way in which the Hund's metal paradigm helps understanding the metallic phases in Fe-based superconductors, hopefully clarifying the ground on which high-Tc superconductivity prospers. We have detailed the way in which realistic DFT+slave-spin mean-field calculations are performed, and how they capture extremely well the behavior of the strong electronic correlations characterizing these phases. We have then exposed the gears inside the calculations, using simplified models—yet having all the essential features of the realistic simulations—in order to show explicitly how Hund's coupling enhances the correlations. We have hopefully given an intuitive justification to its influence that can initially appear counter-intuitive. In particular we have shown how, rather than a simple "arm wrestling" between bare kinetic energy of the electrons and their interaction strength, correlations should be viewed as a result of the available channels for charge fluctuations, and their energy cost, both of which are heavily tuned by Hund's coupling.

Before closing, we should mention that our calculations were all formally done at zero temperature. They are indeed fully representative of the low-but-finite-temperature Fermi-liquid phases encountered in Fe-SC that we have discussed. However more and equally rich Hund's metal physics [18] unveils when raising the temperature, in particular when crossing the Fermi-liquid coherence temperature, both in Fe-SC and in other Hund's metals, and in the related model calculations [2].

Furthermore, we have not even tried to touch upon other crucial aspects of the physics of Fe-SC that are impacted by Hund's coupling. The magnetic phases found in these materials are influenced by the balance between Hund's coupling and non-local exchange mechanisms, while nematicity [19] and superconductivity [20–22] might be amplified by Hund's metal correlations. Some of these aspects are still an ongoing research frontier, and could be interesting material for a future lecture.

References

[1] Z.P. Yin, K. Haule, and G. Kotliar, Nat. Mater. **10**, 932 (2011)

[2] A. Georges and G. Kotliar, Physics Today **77**, 46 (2024)

[3] A. Georges, L. de' Medici, and J. Mravlje,
Annu. Rev. Condens. Matter Physics **4**, 137 (2013)

[4] N. Marzari, A.A. Mostofi, J.R. Yates, I. Souza, and D. Vanderbilt,
Rev. Mod. Phys. **84**, 1419 (2012)

[5] A.V. Chubukov and P.J. Hirschfeld, Physics Today **68**, 46 (2015)

[6] Q. Si and N.E. Hussey, Physics Today **76**, 34 (2023)

[7] F. Hardy, A.E. Böhmer, L. de' Medici, M. Capone, G. Giovannetti, R. Eder, L. Wang,
M. He, T. Wolf, P. Schweiss, R. Heid, A. Herbig, P. Adelmann, R.A. Fisher, and
C. Meingast, Phys. Rev. B **94**, 205113 (2016)

[8] P. Villar Arribi: *Heavy fermions and Hund's metals in iron-based superconductors*
(Ph.D. thesis, Université Grenoble Alpes, 2018)
`https://theses.hal.science/tel-02151075/`

[9] T. Gorni, P. Villar Arribi, M. Casula, and L. de' Medici, Phys. Rev. B **104**, 014507 (2021)

[10] T. Miyake, K. Nakamura, R. Arita, and M. Imada, J. Phys. Soc. Jpn. **79**, 044705 (2010)

[11] M. Crispino, M. Chatzieleftheriou, T. Gorni, and L. de' Medici,
Phys. Rev. B **107**, 155149 (2023)

[12] L. Fanfarillo and E. Bascones, Phys. Rev. B **92**, 075136 (2015)

[13] L. de' Medici and M. Capone: *Modeling Many-Body Physics with Slave-Spin Mean-Field:
Mott and Hund's Physics in Fe-Superconductors* (Springer, Cham, 2017), pp. 115–185.

[14] L. de' Medici, in preparation (2025)

[15] M. Chatzieleftheriou, M. Berović, P. Villar Arribi, M. Capone, and L. de' Medici,
Phys. Rev. B **102**, 205127 (2020)

[16] O. Gunnarsson, E. Koch, and R.M. Martin, Phys. Rev. B **54**, R11026 (1996)

[17] L. de' Medici, J. Mravlje, and A. Georges, Phys. Rev. Lett. **107**, 256401 (2011)

[18] P. Werner, E. Gull, M. Troyer, and A.J. Millis, Phys. Rev. Lett. **101**, 166405 (2008)

[19] L. Fanfarillo, G. Giovannetti, M. Capone, and E. Bascones,
Phys. Rev. B **95**, 144511 (2017)

[20] L. de' Medici, Phys. Rev. Lett. **118**, 167003 (2017)

[21] S. Hoshino and P. Werner, Phys. Rev. Lett. **115**, 247001 (2015)

[22] L. Fanfarillo, A. Valli, and M. Capone, Phys. Rev. Lett. **125**, 177001 (2020)